Chemical Engineering Science 313 (2025) 121759

Contents lists available at ScienceDirect

Chemical Engineering Science

journal homepage: www.elsevier.com/locate/ces

Exploring the role of temperature on hydrotropy

Dinis O. Abranches [a], Bruna P. Soares [a], Isabella W. Cordova [a,b], Jordana Benfica [a], Olga Ferreira [b], Simão P. Pinho [b], João A.P. Coutinho [a,*]

[a] CICECO – Aveiro Institute of Materials, Department of Chemistry, University of Aveiro, Aveiro, Portugal
[b] CIMO-Centro de Investigação de Montanha, LA SusTEC, Instituto Politécnico de Bragança, Campus de Santa Apolónia, 5300-253 Bragança, Portugal

ARTICLE INFO

Keywords:
Green Chemistry
Solvation
Hydrotropes
Hydrophobic Effect
Thermodynamics
Machine Learning

ABSTRACT

Aqueous solubility can be enhanced through hydrotropy, where an amphiphilic molecule (the hydrotrope) aggregates around the solute, boosting its solubility. To understand the impact of temperature on this phenomenon, the solubility of syringic acid was measured in aqueous solutions of different bio-based hydrotropes. Solubility curves were modelled using Gaussian processes, a powerful class of machine learning interpolators. This allowed for a thermodynamic analysis of excess solvation properties that was complemented using the COSMO-RS model.

As expected, the absolute solubility of syringic acid increased with temperature. However, at low hydrotrope concentrations, this increase was not driven by interactions in the liquid phase. Thus, the solubility enhancement of syringic acid was found to be independent of temperature. Conversely, at high hydrotrope concentrations, increasing the temperature significantly decreased the solubility enhancement of the solute. These effects were interpreted considering different solubilization mechanisms, namely hydrotropy (low hydrotrope concentrations) and co-solvency (high hydrotrope concentrations).

1. Introduction

Despite the ongoing search for novel green solvents, which includes, among many other examples, deep eutectic (Hansen et al., 2021), supercritical (Khaw et al., 2017); and bio-based solvents (Calvo-Flores et al., 2018), water remains the most sustainable option (Lajoie et al., 2022; Zhou et al., 2019). Although its large heat capacity and enthalpy of vaporization can lead to significant energy costs in separation processes, particularly those based on vapor–liquid equilibrium (e.g., evaporation or distillation), water is inexpensive and abundant, non-toxic, non-flammable, and overall environmentally benign. Unfortunately, many chemical compounds exhibit poor aqueous solubility and, thus, cannot be dissolved and processed using water. This limitation can be addressed using hydrotropes, compounds that can enhance the solubility of hydrophobic substances in water (Häckl and Kunz, 2018).

Hydrotropy is a thermodynamic phenomenon where the aqueous solubility of a hydrophobic solute is significantly increased in the presence of a small, amphiphilic additive, commonly referred to as the hydrotrope (Patel and Desai, 2023; Kunz et al., 2016). Hydrotrope molecules are smaller than surfactants, and their mechanism of action does not involve the formation of micelles (Shimizu and Matubayasi, 2016). Instead, hydrotropes aggregate around the apolar moieties of solutes (Abranches et al., 2020; Shimizu, 2020). This aggregation, driven by the hydrophobic effect, is more disorganized than complexation or micellization. By reducing the number of contacts between water and the apolar moieties of solute molecules, hydrotropes maximize the hydrogen bonding network of water with itself, thereby enhancing the solubility of the hydrophobic solute. As such, well-designed and appropriately applied hydrotropic systems provide a green and sustainable alternative for industrial processes involving the dissolution of hydrophobic compounds.

Several amphiphilic compounds that exhibit hydrotropic behavior have been extensively studied. Amongst the most popular choices are sodium salts containing aromatic anions, including, for example, sodium benzoate, sodium salicylate, sodium benzenesulfonate, and sodium p-toluenesulfonate (Patel and Desai, 2023; Zakharova et al., 2023; Dhapte and Mehta, 2015; Sales et al., 2022). Their popularity might stem from the incorrect assumption that π-π interactions play an important role in the mechanism of hydrotropy, a notion that has largely been disproven (Shimizu and Matubayasi, 2016; Abranches et al., 2020; Shimizu, 2020). There are also many options for well-studied non-ionic hydrotropes, such as urea or nicotinamide (Dhapte and Mehta, 2015; Booth et al., 2015). More recently, numerous bio-based solvents have also been shown to be excellent hydrotropes. These include ionic liquids (Sintra

* Corresponding author.
E-mail address: jcoutinho@ua.pt (J.A.P. Coutinho).

https://doi.org/10.1016/j.ces.2025.121759
Received 19 March 2025; Received in revised form 24 April 2025; Accepted 28 April 2025
Available online 1 May 2025
0009-2509/© 2025 The Author(s). Published by Elsevier Ltd. This is an open access article under the CC BY license (http://creativecommons.org/licenses/by/4.0/).

et al., 2021; Becker et al., 2021), glycerol ethers (Soares et al., 2020), alkanediols (Abranches et al., 2022), and even dihydrolevoglucosenone (Cyrene) (De bruyn et al., 2019; Abranches et al., 2020).

Trends and relationships between the solubility enhancement of hydrophobic solutes and the nature and composition of hydrotropes are well understood. These include, for instance, the fact that hydrotropes with larger apolar volumes tend to display better hydrotropic efficiency, that increasing hydrotrope concentration increases solubility enhancement up to a specific limit, and that more hydrophobic substances typically experience greater solubility enhancements (Patel and Desai, 2023; Shimizu and Matubayasi, 2016; Abranches et al., 2020; Shimizu, 2020; Booth et al., 2015; Abranches et al., 2022; Abranches et al., 2020). However, very little is known about the impact of temperature on hydrotropy. While it is generally assumed that temperature ubiquitously increases the solubility of solutes, its effect on the hydrophobic effect—an entropically-driven phenomenon—is not as well understood. This implies that temperature may unexpectedly influence the ability of hydrotropes to solvate hydrophobic substances. This topic has seen only limited interest (Shimizu and Matubayasi, 2024) despite the ongoing debates in the literature regarding the molecular mechanisms underlying hydrotropy.

Understanding the impact of temperature on hydrotropy has several advantages beyond the fundamental knowledge gained. For instance, it enables the correct formulation of hydrotrope-solute pairs tailored to specific temperature conditions and developing temperature-swing-based separation processes. Thus, this work aims to study the impact of temperature on hydrotropy. This was done by measuring the aqueous solubility of a hydrophobic solute (syringic acid) in aqueous hydrotropes (bio-based compounds) at different concentrations and temperatures. Syringic acid was selected due to its well-known and studied behavior in the presence of hydrotropes and being a model molecule for lignin and aromatic compounds in waste valorization processes. Bio-based compounds were chosen for their sustainable nature and the extensive research in the literature regarding their standalone usage as solvents or as hydrotropes when dissolved in water. The data obtained was fitted using Gaussian processes (GPs) and further subjected to a thermodynamic analysis that was complemented with thermodynamic models such as COSMO-RS.

2. Materials and methods

2.1. Chemical substances

The chemical substances employed in this work are listed in Table 1, which includes their molar mass, CAS number, source, and mass purity.

Table 1
List of chemical substances experimentally used in this work, including their CAS number, molar mass, source, and purity.

Name	CAS Number	M /g•mol^{-1}	Source	Purity (wt%)
1,2-Propanediol	57-55-6	76.09	Sigma-Aldrich	99.5
1,3-Butanediol	107-88-0	90.12	Sigma-Aldrich	99.5
1,2-Pentanediol	5343-92-0	104.15	TCI	97.0
3-Methoxypropan-1,2-diol ([1.0.0])	623-39-2	106.12	Synthesized[a]	>99.0
2-Ethoxyethanol	110-80-5	90.12	Acros Organics	99.0
Dihydrolevoglucosenone (Cyrene)	53716-82-8	128.13	Sigma-Aldrich	99.0
Syringic Acid	530-57-4	198.17	Acros Organics	>98.0

[a] Part of a batch synthesized in previous works (Abranches et al., 2020; Soares et al., 2020).

The chemical structures of these substances are illustrated in Fig. S1. Water was double distilled, passed through a reverse osmosis system, and further treated with a Milli-Q plus 185 water purification apparatus.

2.2. Solubility measurements

The solubility of syringic acid in binary mixtures of water and various bio-based solvents, namely 1,2-propanediol, 1,3-butanediol, 1,2-pentanediol, [1.0.0], 2-ethoxyethanol, and Cyrene was experimentally measured in this work at atmospheric pressure and different temperatures, ranging from 278.2 K to 343.2 K, using the analytical isothermal shake-flask methodology (Hefter and Tomkins, 2003). To do so, syringic acid was added in slight excess of the expected solubility limit to each hydrotrope solution or pure compound. The samples were equilibrated in an air oven at (303.2 ± 0.5) K under constant stirring (1800 rpm) using an Eppendorf Thermomixer Comfort equipment. After at least 72 h (with thermodynamic equilibrium at higher temperatures requiring up to 120 h of stirring), the liquid phase samples were carefully collected, filtered using syringe filters, and diluted in ultra-pure water. The concentration of syringic acid was then quantified by UV-spectroscopy using a SHIMADZU UV-1700 Pharma-Spec spectrometer at 267 nm.

2.3. Thermodynamic modelling

The solubility of a compound (solute, s) in a given solvent is governed by the solid–liquid equilibrium (SLE) established between the solid phase of the solute and the liquid phase of the solvent. This SLE is typically of the eutectic type and, after some reasonable assumptions, can be described as (Richard Elliott and Lira, 2012):

$$\ln(x_S\gamma_s) = \frac{\Delta_m h_s}{R}\left(\frac{1}{T_{m,s}} - \frac{1}{T}\right) \quad (1)$$

where x_S and γ_s are the mole fraction (solubility) and the activity coefficient of the solute in the liquid phase, respectively, $T_{m,s}$ and $\Delta_m h_s$ are the solute melting temperature and enthalpy, T is the absolute temperature of the system, and R is the ideal gas constant. Note that Equation (1) allows for determining activity coefficients from experimental (x_S, T) solubility data. The melting properties of syringic acid used in this work were taken from the literature (melting temperature, 480.3 K, and melting enthalpy, 33.7 kJ/mol) (Queimada et al., 2009).

COSMO-RS (conductor like screening model for real solvents) is a statistical thermodynamics model capable of predicting the activity coefficients of all components in a liquid mixture without the need for experimental data (Klamt, 1995; Klamt et al., 1998; Eckert and Klamt, 2002). To do so, the model relies on the screened charges of molecules, obtained through quantum chemistry calculations, to estimate the pairwise interaction strength between mixture components. COSMO-RS was used in this work to obtain estimates for the activity coefficients of water, hydrotropes, and syringic acid (allowing for the calculation of syringic acid solubility through Equation (1) in an iterative fashion), as well as their temperature dependencies. As such, all molecules studied in this work were optimized in the quantum chemistry software package TURBOMOLE (TURBOMOLE V7.1, 2016) with a BP-86 functional, the def-TZVP basis set, and the COSMO solvation model with infinite permittivity. The software package COSMOtherm (BIOVIA COSMOtherm, Release, 2021) was used for all COSMO-RS calculations using the BP_TZVP_21 parametrization.

Given that solubility can be treated as a solid–liquid equilibrium, with an equilibrium constant equal to x_S, the van't Hoff equation may be employed to determine the so-called solute enthalpy ($\Delta_d h_s$) and entropy ($\Delta_d s_s$) of solution (Grant et al., 1984; Carrero, 2024):

$$\ln(x_S) = -\frac{\Delta_d h_s}{R} \bullet \frac{1}{T} + \frac{\Delta_d s_s}{R} \quad (2)$$

This is achieved by fitting straight lines to experimental solubility data – $\ln(x_S)$ vs. T^{-1} – and obtaining the slope and intercept. Volumetric units (solubility of syringic acid in g/L) were converted to mole fractions. The densities of the pure solvents at different temperatures were taken from the literature and fitted with a quadratic polynomial. These correlations are reported in Table S1. Densities for the mixtures were obtained assuming thermodynamic ideality.

2.4. Gaussian processes

GPs are a class of stochastic machine learning models that excel at interpolating data across multiple dimensions (i.e., input variables) (Seeger, 2004; Deringer et al., 2021). Among many advantages over other models, GPs are non-parametric, meaning they can describe complex relationships between features (input variables) and labels (output variables) without needing to select a specific functional form for the model. In this work, GPs were employed to describe the solubility of syringic acid as a function of temperature and solvent composition. For each hydrotropic system of interest, a surrogate function representing syringic acid solubility, here denoted as $S'(\boldsymbol{x})$, was constructed and distributed as a GP with a mean function $m(\boldsymbol{x})$ and a covariance function $k(\boldsymbol{x})$ (Rasmussen and Processes, 2004):

$$S'(\boldsymbol{x})\ GP(m(\boldsymbol{x}), k(\boldsymbol{x}))\tag{3}$$

where $\boldsymbol{x} = [\boldsymbol{w}, T]$, with $\boldsymbol{w}$ representing the weight fraction composition of the solvent.

The mean and covariance functions represent intrinsic properties of the relationship between solubility and composition/temperature. In practical applications, the mean function is typically zero, (Deringer et al., 2021) i.e. $m(\boldsymbol{x}) = 0$, which has been shown to be effective in predicting the aqueous solubility of various solutes using GPs (Abranches et al., 2024). Regarding the covariance function, also denoted as the kernel, the popular Matérn 3/2 was selected for this work due to its generality, minimal number of hyperparameters, and differentiability. This kernel is defined as (Duvenaud, 2014; Matthews et al., 2017):

$$k(\boldsymbol{x}_i, \boldsymbol{x}_j) = \sigma^2\left(1+\frac{\sqrt{3}\,\|\boldsymbol{x}_i-\boldsymbol{x}_j\|}{l}\right)\exp\left(-\frac{\sqrt{3}\,\|\boldsymbol{x}_i-\boldsymbol{x}_j\|}{l}\right)\tag{4}$$

where σ^2 and l are the variance and length scale hyperparameters of the kernel, respectively, and $\|\boldsymbol{x}_i - \boldsymbol{x}_j\|$ represents the Euclidian distance between $\boldsymbol{x}_i$ and $\boldsymbol{x}_j$, with i and j being any two datapoints. To directly account for experimental uncertainty, a white noise kernel, k_W, was also added to Equation (4), being defined as (Duvenaud, 2014; Matthews et al., 2017):

$$k_W(\boldsymbol{x}_i, \boldsymbol{x}_j) = \delta(i,j)\sigma_W^2\tag{5}$$

where σ_W^2 is the white noise kernel variance and $\delta(i,j)$ is one when $i = j$ and zero otherwise.

Given a set of N training data points, $(\boldsymbol{x}_i, S_i)$, a new solubility data point S^* associated to $\boldsymbol{x}^*$ (i.e., a testing data point) is said to be jointly distributed as follows:

$$\begin{bmatrix} S_1 \\ \vdots \\ S_N \\ S^* \end{bmatrix} \mathcal{N}(0,\boldsymbol{\Sigma}) = \mathcal{N}\left(0, \begin{bmatrix} \boldsymbol{\Sigma}_{S,S} = \begin{bmatrix} k(\boldsymbol{x}_1,\boldsymbol{x}_1) & \cdots & k(\boldsymbol{x}_1,\boldsymbol{x}_N) \\ \vdots & \ddots & \vdots \\ k(\boldsymbol{x}_N,\boldsymbol{x}_1) & \cdots & k(\boldsymbol{x}_N,\boldsymbol{x}_N) \end{bmatrix} & \boldsymbol{\Sigma}_{S,S^*} = \begin{bmatrix} k(\boldsymbol{x}_1,\boldsymbol{x}^*) \\ \vdots \\ k(\boldsymbol{x}_N,\boldsymbol{x}^*) \end{bmatrix} \\ \boldsymbol{\Sigma}_{S,S^*}^{\boldsymbol{T}} = [\,k(\boldsymbol{x}^*,\boldsymbol{x}_1) & \cdots & k(\boldsymbol{x}^*,\boldsymbol{x}_N)\,] & \boldsymbol{\Sigma}_{S^*,S^*} = k(\boldsymbol{x}^*,\boldsymbol{x}^*) \end{bmatrix}\right)\tag{6}$$

where $\mathcal{N}(0,\boldsymbol{\Sigma})$ represents a multivariate Gaussian distribution with a covariance matrix $\boldsymbol{\Sigma}$, which contains the covariances between training data points ($\boldsymbol{\Sigma}_{S,S}$), testing data points ($\boldsymbol{\Sigma}_{S^*,S^*}$) and cross-covariances ($\boldsymbol{\Sigma}_{S,S^*}$ and $\boldsymbol{\Sigma}_{S,S^*}^{\boldsymbol{T}}$). Thus, treating S^* as a random variable and considering Bayes' theorem (Rasmussen and Processes, 2004):

$$S^*|\boldsymbol{S}\ \mathcal{N}(\mu', \Sigma')\tag{7}$$

with μ' and Σ' being:

$$\mu' = \boldsymbol{\Sigma}_{S,S^*}^{\boldsymbol{T}}\boldsymbol{\Sigma}_{S,S}^{-1}\boldsymbol{S}\tag{8}$$

$$\Sigma' = \boldsymbol{\Sigma}_{S^*,S^*} - \boldsymbol{\Sigma}_{S,S^*}^{\boldsymbol{T}}\boldsymbol{\Sigma}_{S,S}^{-1}\boldsymbol{\Sigma}_{S,S^*}\tag{9}$$

Within the framework of GPs, μ' (Equation (8) represents the GP-predicted solubility value S^* at testing point $\boldsymbol{x}^*$, and Σ' (Equation (9) represents the GP-predicted uncertainty (variance) of this estimate.

GPs were trained and employed in this work using the Python packages GPFlow (Matthews et al., 2017) (V. 2.9.2) and TensorFlow (Abadi et al., 2015) (V. 2.12.1). Kernel hyperparameters and the model Gaussian likelihood were optimized by maximizing the log marginal likelihood of each GP using the L-BFGS-B algorithm (Byrd et al., 1995). Features and labels were normalized following standard procedures in the literature, particularly where aqueous solubilities are successfully predicted (Abranches et al., 2024). Specifically, features and labels were normalized using min–max scaling (Equation (10) and log-standardization (Eq. (11), respectively:

$$z' = \frac{z - z_{min}}{z_{max} - z_{min}}\tag{10}$$

$$z' = \frac{\ln(z) - \langle\ln(z)\rangle}{s_{\ln(z)}}\tag{11}$$

where z' is the normalized version of z, z_{min} and z_{max} are the minimum and maximum values of z, and $\langle\ln(z)\rangle$ and $s_{\ln(z)}$ represent the mean and standard deviation of the transformed variable $\ln(z)$, respectively.

3. Results and discussion

3.1. Solubility curves

The solubility of syringic acid in aqueous mixtures of hydrotropes was measured in this work at various temperatures, ranging from 278.2 K to 342.2 K, and at different hydrotrope concentrations, from pure water to pure hydrotrope. The results, including associated experimental standard deviations, are reported in Tables S2 and S3 of Supporting Information. This data is also depicted in Fig. 1 in the form of solute solubility (g/L) as a function of hydrotrope composition (solute-free basis weight fraction).

Fig. 1 reveals that all amphiphilic molecules (i.e., hydrotropes) explored in this work can significantly enhance the aqueous solubility of syringic acid. In general terms and considering the entire composition range of the water/hydrotrope mixtures, 2-ethoxyethanol is the most effective hydrotrope, increasing the solubility of syringic acid up to 260 g/L at 343 K (compared to 7.6 g/L at the same temperature for pure water without hydrotrope). This is followed by Cyrene (209 g/L),

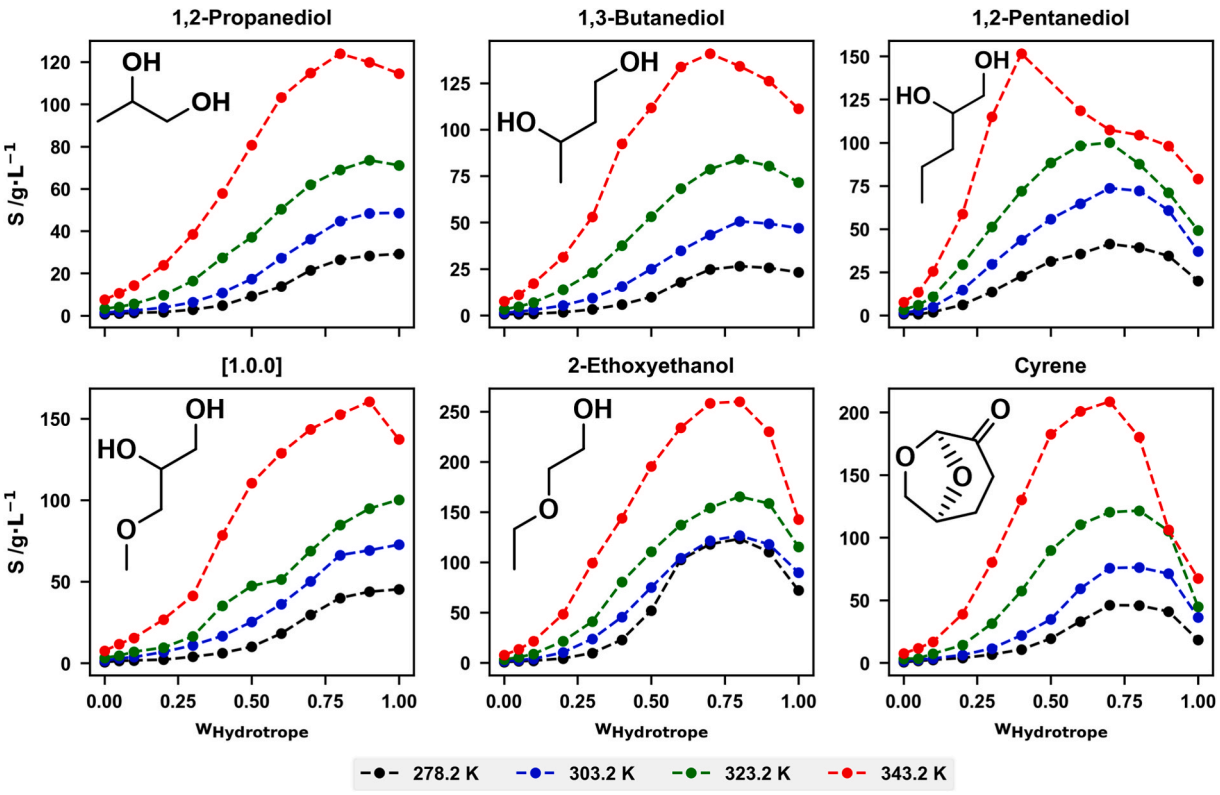

Fig. 1. Solubility (mass of solute per volume of solution) of syringic acid in aqueous hydrotrope solutions as a function of the solute-free basis weight fraction of the hydrotrope. Each panel depicts different hydrotropes, circles represent experimental data measured in this work, and colors represent different temperatures. Lines are simple visual aids. The chemical structures of the hydrotropes are also shown.

[1.0.0] (160 g/L), 1,2-pentanediol (155 g/L), 1,3-butanediol (141 g/L), and, lastly, 1,2-propanediol (124 g/L). These performances are, however, influenced by both temperature and hydrotrope composition.

The solubility curves discussed above are also depicted in Fig. S2, organized by temperature rather than hydrotrope to provide a more comprehensive comparison between hydrotropes. While 2-ethoxyethanol exhibits the most remarkable ability to enhance the aqueous solubility of syringic acid across the entire water/hydrotrope composition range, this is not true at low hydrotrope concentrations. The results depicted in Fig. S2 indicate that 1,2-pentanediol outperforms 2-ethoxyethanol up to a hydrotrope weight percentage of approximately 40 %, regardless of temperature. Furthermore, in this low concentration regime (below 40 %), the performance of hydrotropes can be ranked, from best to worst, as follows: 1,2-pentanediol > 2-ethoxyethanol > Cyrene > 1,3-butanediol > [1.0.0] > 1,2-propanediol. This ordering differs significantly from that listed in the previous paragraph, suggesting a change in the solubilization mechanism of these systems around a weight percentage of 40 %.

As discussed in the Introduction section, hydrotropy is driven by the hydrophobic effect, which leads to the aggregation of apolar hydrotrope moieties around solute molecules. As such, the performance of hydrotropes is closely related to the volume of their apolar moieties (sometimes referred to as their apolarity). This apolar volume (and its availability to aggregate around a solute) can be quantified using quantum-chemistry-derived metrics such as the apolar factor (Abranches et al., 2020) or empirical approaches such as octanol–water partition coefficients (Abranches et al., 2020). When dealing with simple families of similarly structured hydrotropes, molar mass or the number of apolar functional groups can also be used as a metric (Abranches et al., 2022). In this work, apolar volume was loosely quantified by the number of apolar hydrogens in any given hydrotrope. Thus, the apolar volume of the hydrotropes discussed above can be ordered as: 1,2-pentanediol (10 apolar hydrogens) > 2-ethoxyethanol (9) > Cyrene (8) = 1,3-butanediol (8) = [1.0.0] (8) > 1,2-propanediol (6). Note how this closely follows the ranking of best performing hydrotropes below 40 wt %.

The larger the apolar volume of a hydrotrope, the stronger the driving force for solute-hydrotrope aggregation, resulting in better performances. Moreover, a hydrotropy solubilization mechanism is only possible when water is the primary solvent in the system, allowing the hydrophobic effect to occur. Thus, it is unsurprising that the compound with the largest alkyl chain (1,2-pentanediol) exhibits the best hydrotropic performance at low concentrations. The comparison between 1,2-pentanediol and [1.0.0] further underscores the significance of apolarity in hydrotropy. The structures of these two hydrotropes are similar, with one carbon atom in the former being replaced by an oxygen in the latter. This reduction in apolarity leads to a marked decrease in hydrotropic efficiency.

All the above observations support the notion that hydrotropy is the dominant mechanism at hydrotrope weight percentages below 40 wt% for the systems studied in this work. Beyond this concentration, another mechanism, here generically termed co-solvency, becomes predominant. In this regime, water is no longer the dominant solvent in the system, and the hydrophobic effect diminishes in importance when replaced by the solvation in the dominant solvent, i.e., the co-solvent. It is worth noting, though, that Cyrene may have a larger apolar volume than 1,2-pentanediol, depending on how this quantity is defined. Nevertheless, Cyrene establishes a chemical equilibrium in water between its ketone and geminal diol forms. This reactivity with water and change in chemical structure alters the effectiveness of Cyrene as a hydrotrope, as we discussed in detail in previous work (Abranches et al., 2020).

Now focusing on the influence of temperature on hydrotropy, rather than that of composition or hydrotrope structure, the results depicted in Fig. 1 show that an increase in temperature leads to an increase in the solubility of syringic acid across all systems studied. Furthermore,

excepting 1,2-propanediol and [1.0.0] between 278 K and 323 K, all solubility curves display a maximum concerning hydrotrope composition. The position of this maximum tends to shift towards lower hydrotrope concentrations as the temperature increases. Additionally, the onset of the exponential rise in solute solubility, often referred to as the minimum hydrotrope concentration (MHC) in analogy to the critical micellar concentration (CMC) of surfactants, is also observed to decrease with increasing temperature.

Despite the clear differences between hydrotropes and surfactants, the concepts of MHC and CMC are frequently related in the literature (Shimizu and Matubayasi, 2016). As such, it is worth highlighting the similarities in how temperature affects CMCs and MHCs observed in this work. The CMCs of ionic surfactants tend to display non-monotonic behavior with temperature, whereas the CMCs of their non-ionic counterparts tend to decrease as temperature increases (Tadros and Concentration, 2013). For instance, Khoshnood et al. (Khoshnood et al., 2016) showed that the CMCs of sodium dodecyl sulfate, sodium decyl sulfate, sodium tetradecyl sulfate, dodecyl trimethylammonium bromide exhibited an absolute minimum concerning temperature (note the similarity of these surfactants with the ionic hydrotropes mentioned in the Introduction). For all systems studied in this work, which involve only non-ionic hydrotropes, MHCs consistently and monotonically decreased with increasing temperature (Fig. 1), aligning with the behavior observed for non-ionic surfactants.

3.2. Solubility enhancement

As discussed in the previous section, the positive effect of temperature on solubility is a well-established result of basic solid–liquid equilibrium thermodynamics. To better highlight this fundamental relationship between temperature and solubility, remembering the assumption of no solid phase transitions and disregarding the change of the heat capacity upon melting, Equation (1) can be rearranged as:

$$x_S = A\exp\left(-\frac{B}{T}\right) \bullet \frac{1}{\gamma_S} \tag{12}$$

where $A = \exp\left(\frac{\Delta_m h_s}{RT_{m,s}}\right)$ and $B = \frac{\Delta_m h_s}{R}$ are temperature-independent parameters. Note how as the temperature increases, so does the exponential term in Equation (12), leading to a corresponding increase of x_S. This phenomenon is associated with changes in the Gibbs energy of the solid solute and is unrelated to the intermolecular interactions established between the solute and the solvent in the liquid phase, which are described by γ_S.

To understand how temperature influences the aggregation behavior of hydrotropes and solutes in aqueous solutions, or in other words, to study the impact of temperature on hydrotropy, solubility data must be analyzed while removing the effect of temperature on the Gibbs energy of the solid. This can be achieved by examining the so-called solubility enhancement, which quantifies the increase in solubility of a solute upon the addition of a hydrotrope. For any given temperature, solubility enhancement is defined as the ratio between the molar solubility of the solute in the solvent mixture and its molar solubility in pure water, denoted as $S(T)/S_{w_H=0}(T)$. Following Equation (12), this ratio is influenced solely by the activity coefficients of the solute and density changes in the solvent. As such, the solubility curves discussed in the previous section are presented in Fig. 2 as solubility enhancements rather than absolute solubility values. Furthermore, activity coefficients were directly calculated from this experimental solubility data using Equation (1) and are reported in Figs. S3 and S4.

The results depicted in Fig. 2 are remarkable. Surprisingly, temperature does not affect the thermodynamic behavior of hydrotropy. For all systems studied, there is a composition window, from pure water to a hydrotrope weight percentage of approximately 40 % (the exact value varies by hydrotropic system), within which the solubility enhancement

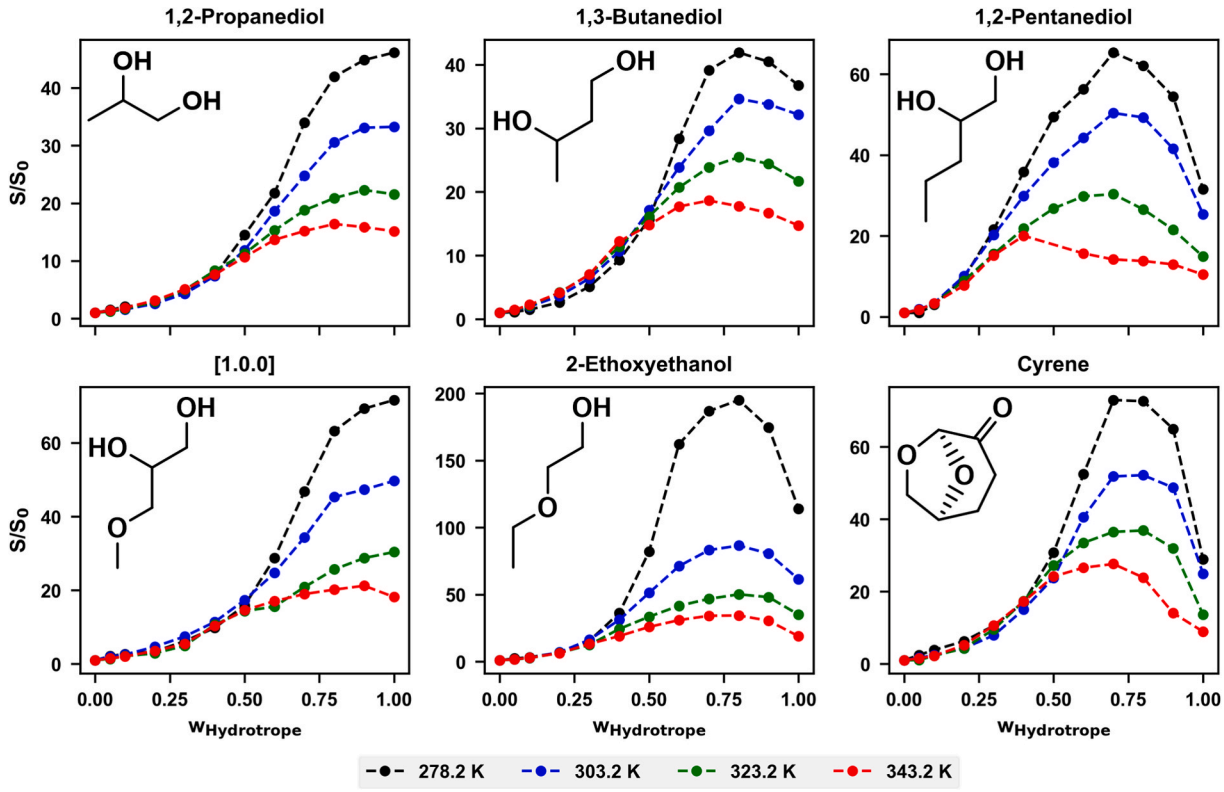

Fig. 2. Solubility enhancement – $S(T)/S_{w_H=0}(T)$ – of syringic acid in aqueous hydrotrope solutions as a function of the solute-free basis weight fraction of the hydrotrope. Each panel depicts different hydrotropes, circles represent experimental data measured in this work, and colors represent different temperatures. Lines are simple visual aids. The chemical structures of the hydrotropes are also shown.

of syringic acid remains unchanged by temperature. Beyond this point, increasing temperature actually leads to a decrease in solubility enhancement. These findings suggest that syringic acid is solubilized by two distinct mechanisms (or regimes), depending on the concentration of the hydrotrope, consistent with the conclusions drawn in the previous section.

The fact that the solubility enhancement of syringic acid remains unaffected by temperature within the hydrotropy regime does not imply that the hydrophobic effect is temperature-independent. The significant influence of temperature on the hydrophobic effect, which drives hydrotropy (Shimizu and Matubayasi, 2016; Abranches et al., 2020), is well-documented (Shimizu and Chan, 2000; Southall et al., 2002; Kronberg et al., 1994). From a molecular mechanistic perspective, even when disregarding entropic effects on apolar-apolar clusters, an increase in temperature weakens the hydrogen bonding network of water due to the increased thermal motion of water molecules, thus altering the driving force of the hydrophobic effect (Swiatla-Wojcik et al., 2008; Dougherty, 1998). Instead, the results presented in Fig. 2 suggest that, within the hydrotropy regime, the impact of temperature on the hydrophobic effect is independent of the hydrotrope concentration. In other words, and because solubility enhancements represent relative ratios taken at the same temperature – $S(T)/S_{w_H=0}(T)$, the intermolecular interactions between syringic acid and pure water or water/hydrotrope mixtures appear to be affected by temperature in the same way. This indicates a thermodynamic process where the entropy contribution to the excess Gibbs free energy is much greater than its enthalpy counterpart. This is related to the hydrotrope-solute interactions being dominated by dispersion forces, which are by nature athermal.

The observation that temperature decreases the solubility enhancement of syringic acid at large hydrotrope concentrations (recall that this composition window is here referred to as the co-solvency regime) is easy to explain. The hallmark of co-solvency is the formation of enthalpically-driven intermolecular interactions, particularly hydrogen bonding, at concentrations where water, in loose terms, is not the primary solvent of the system (Gomes et al., 2024; Andanson et al., 2014; Abranches et al., 2020). As temperature increases, the strength of these interactions diminishes due to the heightened thermal motion of the molecules (Dougherty, 1998). This results in a decrease in the solubility enhancement of syringic acid, as shown in Fig. 2. Additionally, it reduces the activity coefficients, approaching unity (thermodynamic ideality), as illustrated in Figs. S3 and S4.

The discussion above, including the identification of two distinct solubilization mechanisms in the hydrotropic systems studied in this work, is aligned with previous findings in the literature (Abranches et al., 2020; Abranches et al., 2022; Abranches et al., 2020). For example, while Cyrene has been demonstrated to act as a hydrotrope, at high Cyrene concentrations where water is no longer the primary solvent of the system and the hydrophobic effect is absent, water has been shown to mediate hydrogen bonding interactions between syringic acid and Cyrene (Abranches et al., 2020). This phenomenon helps explain why both absolute solubilities and solubility enhancements display a maximum concerning the hydrotrope composition. Thus, paradoxically, water can enhance the solubility of hydrophobic substances in amphiphilic solvents through co-solvency, as will be further explained below.

3.3. COSMO-RS

As mentioned in the Methods section, the thermodynamics model COSMO-RS was employed to predict the solubility of syringic acid in the aqueous solutions of hydrotropes studied in this work across the entire composition and temperature ranges. While the theoretical foundations of this model lie on pair-wise interactions, there is limited evidence in the literature (Abranches et al., 2020) suggesting that COSMO-RS can capture the complex n-body interactions that give rise to the hydrophobic effect and hydrotropy. The results obtained are reported in Fig. 3.

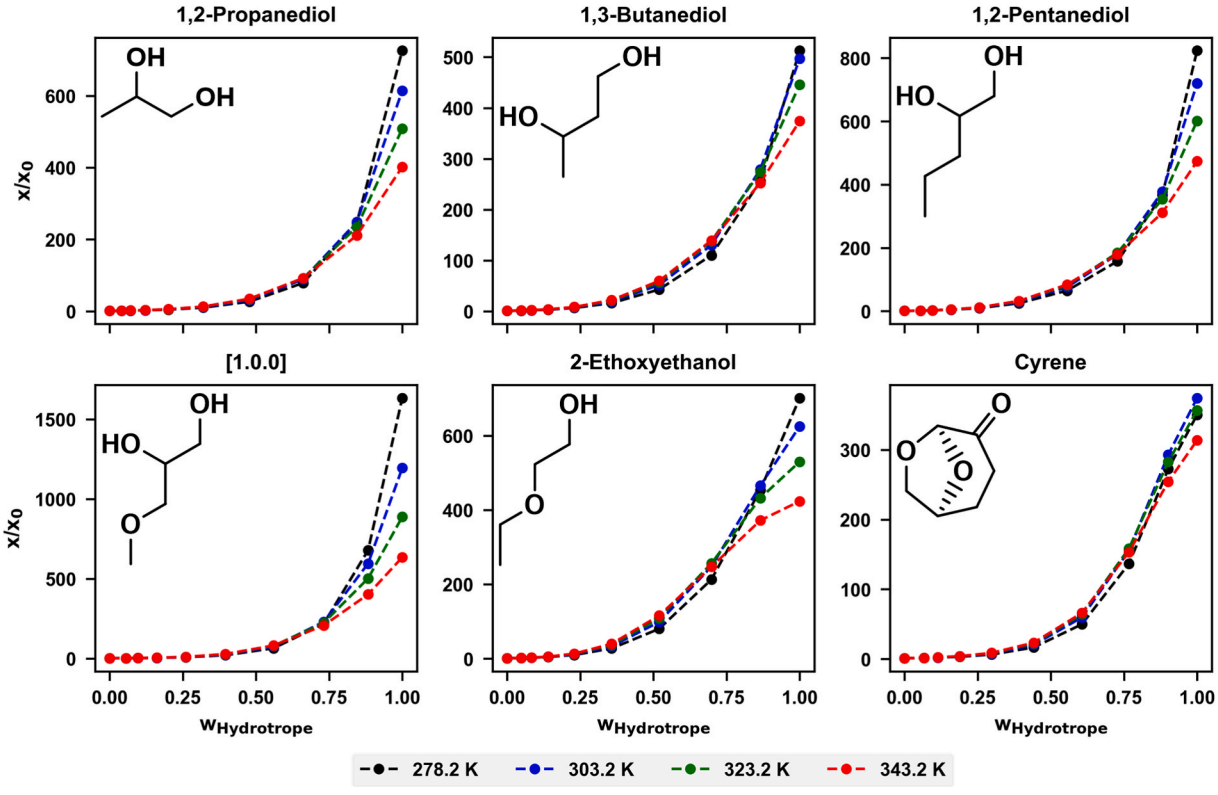

Fig. 3. Solubility enhancement in mole fraction basis – $x(T)/x_{w_H=0}(T)$ – of syringic acid in aqueous hydrotrope solutions as a function of the solute-free basis weight fraction of the hydrotrope, predicted using COSMO-RS Each panel depicts different hydrotropes, circles represent COSMO-RS predictions, and colors represent different temperatures. Lines are simple visual aids. The chemical structures of the hydrotropes are also shown.

COSMO-RS is unable to quantitatively predict the solubility enhancement of syringic acid, with deviations from the experimental values (Fig. 2) exceeding one order of magnitude. Moreover, COSMO-RS does not predict solubility maxima (with respect to hydrotrope composition) in the co-solvency region for any of the systems studied. However, the qualitative trends observed with respect to temperature are interesting. In particular, COSMO-RS indicates that at low hydrotrope concentration (i.e., in the hydrotrope regime), temperature has a negligible impact on solubility enhancement. In contrast, at high hydrotrope concentration (i.e., in the co-solvency regime) temperature negatively impacts solubility enhancement. This fully agrees with the observations made in the previous section, suggesting that COSMO-RS is capturing, albeit qualitatively, the different mechanisms of hydrotropy and co-solvency.

Given the accurate qualitative trends of COSMO-RS described above, this model is now used to examine the molecular mechanism behind the unusual temperature dependencies identified so far. To do so, the mixture of water/1,2-pentanediol was taken as an illustrative example, and the activity coefficients of water were computed, along with the infinite dilution activity coefficients of syringic acid and its excess enthalpy and entropy. These results are depicted in Fig. 4 on a mole basis.

Fig. 4 presents several important results. The activity coefficient of water in the binary water/hydrotrope mixture is, remarkably, constant with respect to temperature until a hydrotrope mole fraction of roughly 0.2. This corresponds roughly to the composition window where the solubility enhancement of syringic acid is constant with temperature and supports the notion raised in the previous section that, in the hydrotropy regime, the impact of temperature on the intermolecular interactions in pure water and water/hydrotrope mixtures is very similar. Surprisingly, within this low hydrotrope composition window, the excess enthalpy of syringic acid at infinite dilution changes considerably with temperature. However, the contribution of its excess entropy counterpart, which does not exhibit such a strong dependency on temperature, is dominant at low hydrotrope concentrations.

The results discussed above also reinforce the two solubility regimes of syringic acid, which COSMO-RS captures qualitatively. At low hydrotrope compositions, the thermodynamic behavior of syringic acid is dominated by entropic factors. Although its excess enthalpy changes with temperature (as expected), its contribution to the final excess Gibbs energy of syringic acid is insignificant. Then, at high hydrotrope compositions, enthalpic contributions become prevalent over their entropic counterparts, signifying a shift from a hydrotropy regime to a co-solvency.

3.4. ML modelling and thermodynamic assessment

A meticulous analysis of the thermodynamic properties of the systems examined in this work, utilizing the van't Hoff approach (Equation (2), may help uncover the molecular mechanisms underlying the unusual temperature trends identified in the previous sections. This analysis is facilitated by having a smooth function directly relating solubility with solvent composition and temperature. To achieve this, a GP model was fitted to each system studied, as detailed in the section on "Gaussian Processes," and the results are reported in Fig. 5. The usage of GPs is based on their exceptional capability to interpolate experimental data while natively handling both experimental and epistemic uncertainty, mitigating the risk of overfitting.

The results presented in Fig. 5 show that GPs can interpolate the solubility of syringic acid across the entire range of compositions and temperatures investigated. The models achieved a relatively low mean relative error (MRE) for each system, with a maximum value of 4.7 % when the hydrotrope is [1.0.0] and an average across all systems of just 2.9 %. Moreover, the main landscape characteristics of each system are well captured, including the presence of solubility maxima and the exponential relationship between solubility and temperature. This demonstrates that GPs serve as a viable alternative to thermodynamic modelling for hydrotropic systems, which is particularly relevant due to a lack of models capable of capturing the composition and temperature trends of these systems.

Having constructed smooth GP models for the solubility of syringic acid with respect to solvent composition and temperature, the en-

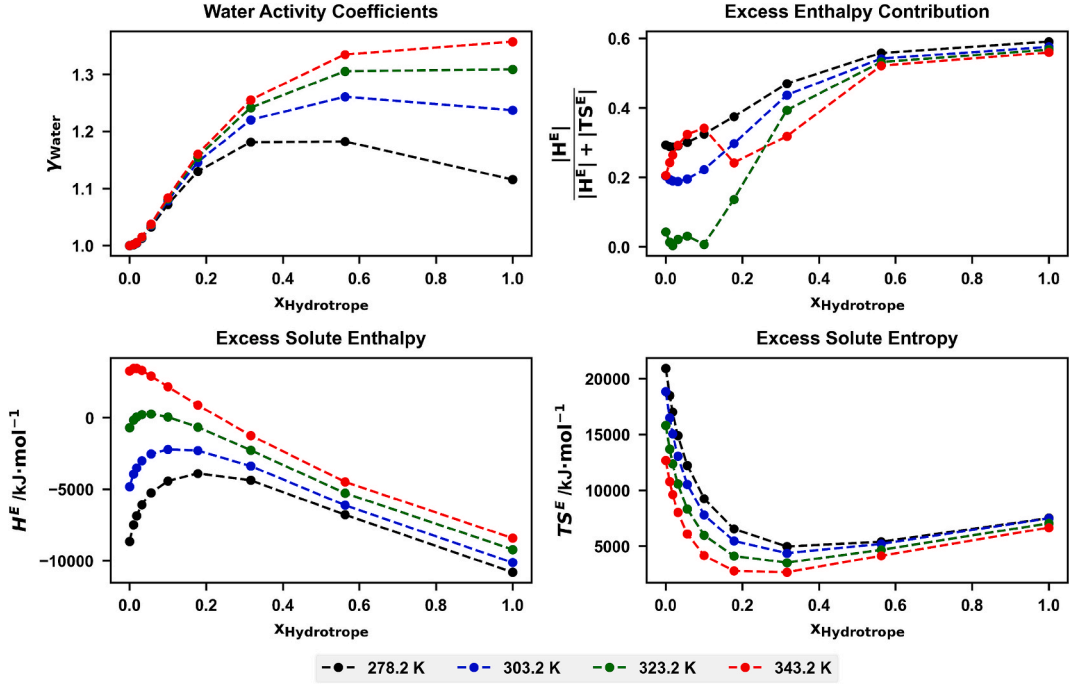

Fig. 4. Predicted activity coefficients of water in the water/1,2-pentanediol binary mixture (top left corner), along with the contribution of excess enthalpy to the excess Gibbs energy (top right corner), excess enthalpies (bottom left corner), and excess entropies (bottom right corner) of syringic acid at infinite dilution. Circles represent COSMO-RS predictions, and colors represent different temperatures. Lines are simple visual aids.

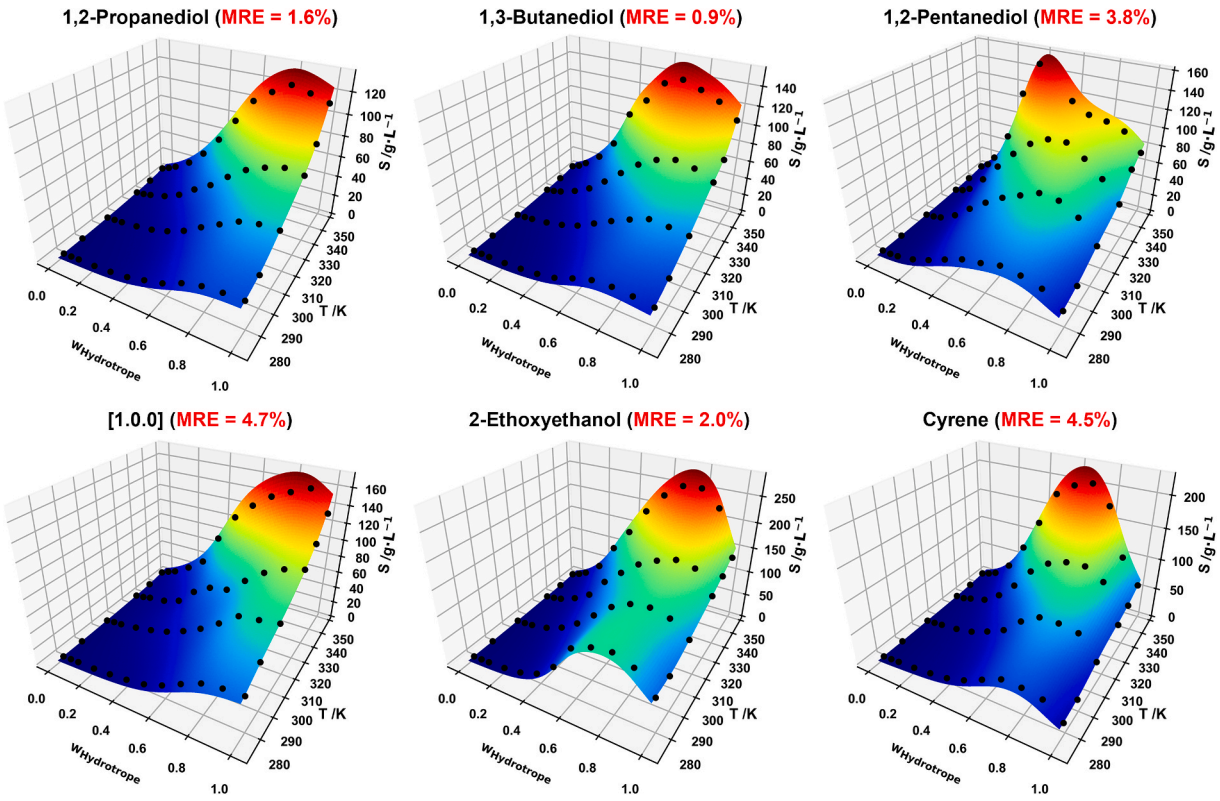

Fig. 5. GP-predicted solubility (mass of solute per volume of solution) of syringic acid in aqueous hydrotrope solutions as a function of the solute-free basis weight fraction of the hydrotrope and temperature. Each panel depicts different hydrotropes, and circles represent experimental data measured in this work. Mean relative errors for the GP-predicted data are also included.

thalpies and entropies of solvation are now estimated for these systems using the van't Hoff approach. To do so, GPs were employed to generate solubility data across 20 different compositions, ranging from pure water to pure hydrotrope, with 20 temperature points per composition within the range 278.2–343.2 K. Then, following the procedure explained above, the enthalpies and entropies of solvation were extracted from the plots of $\ln x_S$ versus $1/T$ by fitting linear polynomials. These plots are depicted in Fig. S5 for select compositions and temperatures.

It is important to note that while the $\ln x_S$ vs. $1/T$ plots depicted in Fig. S5 display strong linear correlations, small variations in $\ln x_S$ can lead to significant changes in the derived enthalpies and entropies of solvation. This is especially true at low hydrotrope concentrations, where the experimental solubility value of syringic acid is small, making it more difficult to have precise solubility measurements. This is why GPs were employed in this work to process the data and prevent a rough and noisy landscape for enthalpy and entropy. Despite these efforts, the accuracy of the determined values for solvation enthalpy and entropy is

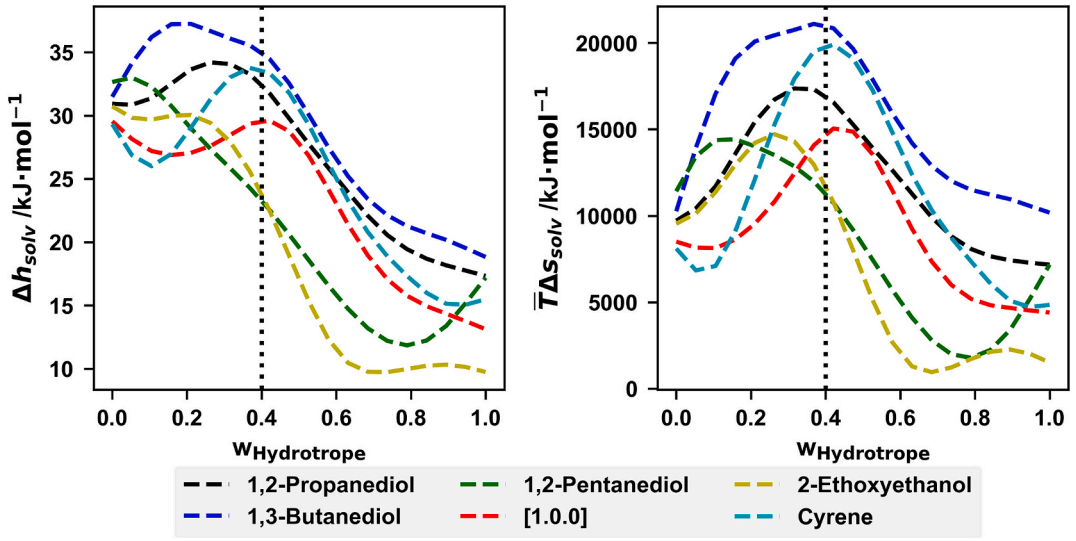

Fig. 6. Enthalpy (left) and entropy (right) of solvation of syringic acid in aqueous hydrotrope solutions as a function of the solute-free basis weight fraction of the hydrotrope, estimated using the van't Hoff approach from GP-predicted data. Vertical dotted lines represent a hydrotrope weight fraction of 0.4.

expected to have high uncertainty. It should be interpreted as indicative of general trends rather than settled values, that can be more correct by calorimetric measurements. The enthalpies and entropies of solvation at different solvent compositions are shown in Fig. 6.

The enthalpy of solvation represents the enthalpy associated with the solvation of syringic acid in water/hydrotrope mixtures. It is a different thermodynamic quantity from the solute excess enthalpy reported in Fig. 4. Its values, reported in Fig. 6, are always positive across the entire composition range of the water/hydrotrope mixtures, indicating a predominantly endothermic solvation process. The enthalpies of solvation around pure water display a value of roughly 30 kJ/mol, similar to that observed in the solvation of alkanes (e.g., 33 kJ/mol for hexane) (Morgado et al., 2020). Moreover, despite their large absolute values, the enthalpies of solvation exhibit minimal variation (less than 15 %) between pure water and approximately 40 % of the hydrotrope mass fraction. Thus, while temperature has a pronounced effect on the absolute solubility of syringic acid within this composition range, as expected from a thermodynamic process with a significantly associated enthalpy, the solubility enhancements remain unaffected by temperature due to the small variations in enthalpy (that is, the enthalpy difference between water/hydrotrope mixtures and pure water govern the impact of temperature on solubility enhancement).

The fact that the enthalpy of solvation does not significantly change within hydrotrope weight percentages of 0–40 % suggests that hydrotrope-solute interactions are essentially athermal, as would be expected since dispersion forces dominate hydrotrope-solute interactions. This observation is consistent with the thermodynamic quantities predicted by COSMO-RS in the previous section, along with the observation that temperature affects the thermodynamic behavior of syringic acid in pure water and in water/hydrotrope mixtures in the same manner. Beyond a hydrotrope weight percentage of 40 %, there is a sharp decrease in the enthalpies of solvation for all systems, particularly within the 40–60 % range. This decrease is related to the transition from a hydrotropy regime to a co-solvency regime, indicating the prevalence of enthalpically-driven solute-hydrotrope interactions and contacts and a more favorable environment for the solute. Note that pure 2-ethoxyethanol presents the lowest enthalpy of solvation, around 10 kJ/mol, which was also the co-solvent that attained the highest solubility enhancement of syringic acid, as explained in the previous sections.

Focusing now on the entropy of solvation, its value in pure water is approximately 30 J/(K•mol), which is somewhat lower than what is observed for common alkanes in water (e.g., 45 J/(K•mol) for hexane) (Morgado et al., 2020). Furthermore, the overall trend with hydrotrope composition differs from that observed for the enthalpy of solvation. Specifically, the entropy of solvation generally increases for all systems until reaching a maximum at around a hydrotrope weight percentage of 40 %, decreasing thereafter. This suggests that the transition from the hydrotropy solubilization regime to the co-solvency regime, when the temperature has a remarkable impact on the solubility enhancement, is associated with a maximum in the entropy value.

4. Conclusions

In this work, the solubility of a hydrophobic compound syringic acid was measured in binary mixtures of water and bio-based solvents at different temperatures and the entire composition range of the solvent, from pure water to pure hydrotrope. The solvents selected, namely 1,2-propanediol, 1,3-butanediol, 1,2-pentanediol, [1.0.0], 2-ethoxyehtanol, and Cyrene are of varying polarities and hydrophobic volumes. The solubility data was analyzed in terms of absolute and relative solubilities alongside predictions with the COSMO-RS thermodynamic model, connecting also to the enthalpies and entropies of solvation, which were obtained employing a thermodynamic approach enhanced by machine learning-smoothed data.

Remarkably, the results obtained and discussed throughout this work reveal that temperature has a negligible effect on the solubility enhancement of syringic acid in the hydrotropy regime (i.e., low hydrotrope concentrations, roughly below 40 wt%). Moreover, the different effects of temperature on the thermodynamic behavior of syringic acid allowed for a clear distinction between hydrotropy and a second solvation regime, termed co-solvency, where increasing temperature decreases the solubility enhancement of syringic acid. These conclusions were made based on the following observations:

i) The bio-based solvent with the largest apolar volume, 1,2-propanediol, is the most effective hydrotrope up to a hydrotrope weight percentage of approximately 40 wt%, beyond which 2-ethoxyethanol becomes more effective.
ii) The impact of temperature on the solubility enhancement of syringic acid differs significantly at hydrotrope compositions below and above approximately 40 wt%.
iii) Syringic acid activity coefficients remain constant with temperature until a hydrotrope weight percentage of 40 wt%, increasing afterwards.
iv) Enthalpies of solvation remain relatively constant up to approximately 40 wt% hydrotrope, after which they sharply decline.
v) Entropies of solvation reach a maximum at approximately 40 wt % of hydrotrope mass percentage.

All in all, while the absolute solubility of syringic acid consistently increased with temperature, the unusual temperature-dependent trends in solubility enhancement, activity coefficients, and thermodynamic properties have enabled the identification of distinct solubilization regimes. These findings highlight the importance of studying hydrotropy, or at least measuring solubility curves, across various temperatures and solvent compositions, as the best solvation additive is not always clear and varies with concentration.

CRediT authorship contribution statement

Dinis O. Abranches: Writing – review & editing, Writing – original draft, Software, Investigation, Data curation, Conceptualization. **Bruna P. Soares:** Writing – original draft, Investigation, Data curation. **Isabella W. Cordova:** Investigation. **Jordana Benfica:** Investigation. **Olga Ferreira:** Supervision, Project administration, Funding acquisition. **Simão P. Pinho:** Writing – review & editing, Supervision, Project administration, Funding acquisition. **João A.P. Coutinho:** Writing – review & editing, Supervision, Resources, Project administration, Funding acquisition, Conceptualization.

Declaration of competing interest

The authors declare that they have no known competing financial interests or personal relationships that could have appeared to influence the work reported in this paper.

Acknowledgments

This work was developed within the scope of the project CICECO-Aveiro Institute of Materials, UIDB/50011/2020 (DOI 10.54499/UIDB/50011/2020), UIDP/50011/2020 (DOI 10.54499/UIDP/50011/2020) & LA/P/0006/2020 (DOI 10.54499/LA/P/0006/2020), and CIMO-Centro de Investigação de Montanha, UIDB/00690/2020 (DOI: 10.54499/UIDB/00690/2020), UIDP/00690/2020 (DOI: 10.54499/UIDP/00690/2020); and SusTEC, LA/P/0007/2020 (DOI: 10.54499/LA/P/0007/2020), all financed by national funds through the FCT/MCTES (PIDDAC).

Appendix A. Supplementary data

Supplementary data to this article can be found online at https://doi.org/10.1016/j.ces.2025.121759.

Data availability

Please see SI.

References

Hansen, B.B., Spittle, S., Chen, B., Poe, D., Zhang, Y., Klein, J.M., Horton, A., Adhikari, L., Zelovich, T., Doherty, B.W., Gurkan, B., Maginn, E.J., Ragauskas, A., Dadmun, M., Zawodzinski, T.A., Baker, G.A., Tuckerman, M.E., Savinell, R.F., Sangoro, J.R., 2021. Deep Eutectic Solvents: A Review of Fundamentals and Applications. Chem. Rev. 121, 1232–1285. https://doi.org/10.1021/acs.chemrev.0c00385.

Khaw, K.-Y., Parat, M.-O., Shaw, P.N., Falconer, J.R., 2017. Solvent Supercritical Fluid Technologies to Extract Bioactive Compounds from Natural Sources: A Review. Molecules 22, 1186. https://doi.org/10.3390/molecules22071186.

Calvo-Flores, F.G., Monteagudo-Arrebola, M.J., Dobado, J.A., Isac-García, J., 2018. Green and Bio-Based Solvents. TOP Curr. Chem. 376, 18. https://doi.org/10.1007/s41061-018-0191-6.

Lajoie, L., Fabiano-Tixier, A.-S., Chemat, F., 2022. Water as green solvent: methods of solubilisation and extraction of natural products—past. Present Future Solutions Pharmaceut. 15, 1507. https://doi.org/10.3390/ph15121507.

Zhou, F., Hearne, Z., Li, C.-J., 2019. Water—the greenest solvent overall. Curr. Opin Green Sustain Chem. 18, 118–123. https://doi.org/10.1016/j.cogsc.2019.05.004.

Häckl, K., Kunz, W., 2018. Some aspects of green solvents. Comptes Rendus. Chimie 21, 572–580. https://doi.org/10.1016/j.crci.2018.03.010.

Patel, A.D., Desai, M.A., 2023. Progress in the field of hydrotropy: mechanism, applications and green concepts. Rev. Chem. Eng. 39, 601–630. https://doi.org/10.1515/revce-2021-0012.

Kunz, W., Holmberg, K., Zemb, T., 2016. Hydrotropes, Curr Opin Colloid. Interface Sci 22, 99–107. https://doi.org/10.1016/j.cocis.2016.03.005.

Shimizu, S., Matubayasi, N., 2016. The origin of cooperative solubilisation by hydrotropes. PCCP 18, 25621–25628. https://doi.org/10.1039/C6CP04823D.

Abranches, D.O., Benfica, J., Soares, B.P., Leal-Duaso, A., Sintra, T.E., Pires, E., Pinho, S. P., Shimizu, S., Coutinho, J.A.P., 2020. Unveiling the mechanism of hydrotropy: evidence for water-mediated aggregation of hydrotropes around the solute. Chem. Commun. 56, 7143–7146. https://doi.org/10.1039/D0CC03217D.

Shimizu, S., 2020. Formulating rationally via statistical thermodynamics, Curr Opin Colloid. Interface Sci. 48, 53–64. https://doi.org/10.1016/j.cocis.2020.03.008.

Zakharova, L.Y., Vasilieva, E.A., Mirgorodskaya, A.B., Zakharov, S.V., Pavlov, R.V., Kashapova, N.E., Gaynanova, G.A., 2023. Hydrotropes: Solubilization of nonpolar compounds and modification of surfactant solutions. J Mol Liq 370, 120923. https://doi.org/10.1016/j.molliq.2022.120923.

Dhapte, V., Mehta, P., 2015. Advances in hydrotropic solutions: An updated review, St. Petersburg Polytechnical University Journal: Physics and Mathematics 1, 424–435. https://doi.org/10.1016/j.spjpm.2015.12.006.

Sales, I., Dinis, O., Abranches, T.E., Sintra, S., Mattedi, M.G., Freire, J.A.P., Coutinho, S.P. P., 2022. Selection of hydrotropes for enhancing the solubility of artemisinin in aqueous solutions. Fluid Phase Equilib 562, 113556. https://doi.org/10.1016/j.fluid.2022.113556.

Booth, J.J., Omar, M., Abbott, S., Shimizu, S., 2015. Hydrotrope accumulation around the drug: the driving force for solubilization and minimum hydrotrope concentration for nicotinamide and urea. PCCP 17, 8028–8037. https://doi.org/10.1039/C4CP05414H.

Sintra, T.E., Abranches, D.O., Benfica, J., Soares, B.P., Ventura, S.P.M., Coutinho, J.A.P., 2021. Cholinium-based ionic liquids as bioinspired hydrotropes to tackle solubility challenges in drug formulation. Eur. J. Pharm. Biopharm. 164, 86–92. https://doi.org/10.1016/j.ejpb.2021.04.013.

Becker, M., Rentsch, D., Reber, D., Aribia, A., Battaglia, C., Kühnel, R., 2021. The hydrotropic effect of ionic liquids in water-in-salt electrolytes. Angew. Chem. Int. Ed. 60, 14100–14108. https://doi.org/10.1002/anie.202103375.

Soares, B.P., Abranches, D.O., Sintra, T.E., Leal-Duaso, A., García, J.I., Pires, E., Shimizu, S., Pinho, S.P., Coutinho, J.A.P., 2020. Glycerol ethers as hydrotropes and their use to enhance the solubility of phenolic acids in water. ACS Sustain. Chem. Eng. 8, 5742–5749. https://doi.org/10.1021/acssuschemeng.0c01032.

Abranches, D.O., Soares, B.P., Ferreira, A.M., Shimizu, S., Pinho, S.P., Coutinho, J.A.P., 2022. The impact of size and shape in the performance of hydrotropes: a case-study of alkanediols. PCCP 24, 7624–7634. https://doi.org/10.1039/D2CP00496H.

De bruyn, M., Budarin, V.L., Misefari, A., Shimizu, S., Fish, H., Cockett, M., Hunt, A.J., Hofstetter, H., Weckhuysen, B.M., Clark, J.H., Macquarrie, D.J., 2019. Geminal Diol of Dihydrolevoglucosenone as a Switchable Hydrotrope: a Continuum of Green Nanostructured Solvents. ACS Sustain Chem Eng 7, 7878–7883. https://doi.org/10.1021/acssuschemeng.9b00470.

Abranches, D.O., Benfica, J., Shimizu, S., Coutinho, J.A.P., 2020. The perspective of cooperative hydrotropy on the solubility in aqueous solutions of cyrene. Ind. Eng. Chem. Res. 59, 18649–18658. https://doi.org/10.1021/acs.iecr.0c02346.

Shimizu, S., Matubayasi, N., 2024. Temperature dependence of hydrotropy. J. Phys. Chem. B 128, 10915–10924. https://doi.org/10.1021/acs.jpcb.4c04619.

G.T. Hefter, R.P.T. Tomkins, eds., The Experimental Determination of Solubilities, Wiley, 2003. https://doi.org/10.1002/0470867833.

Richard Elliott, J., Lira, C.T., 2012. Introductory Chemical Engineering Thermodynamics, 2nd ed.,. Prentice Hall, Upper Saddle River, NJ.

Queimada, A.J., Mota, F.L., Pinho, S.P., Macedo, E.A., 2009. Solubilities of Biologically Active Phenolic Compounds: Measurements and Modeling. J. Phys. Chem B 113, 3469–3476. https://doi.org/10.1021/jp808683y.

Klamt, A., 1995. Conductor-like Screening Model for Real Solvents: A New Approach to the Quantitative Calculation of Solvation Phenomena. J. Phys. Chem 99, 2224–2235. https://doi.org/10.1021/j100007a062.

Klamt, A., Jonas, V., Bürger, T., Lohrenz, J.C.W., 1998. Refinement and Parametrization of COSMO-RS. J. Phys. Chem A 102, 5074–5085. https://doi.org/10.1021/jp980017s.

Eckert, F., Klamt, A., 2002. Fast solvent screening via quantum chemistry: COSMO-RS approach. AIChE J 48, 369–385. https://doi.org/10.1002/aic.690480220.

TURBOMOLE V7.1 2016, a development of University of Karlsruhe and Forschungszentrum Karlsruhe GmbH, 1989-2007, TURBOMOLE GmbH, since 2007; available from \\ http://www.turbomole.com., (n.d.).

BIOVIA COSMOtherm, Release 2021, (n.d.).

Grant, D.J.W., Mehdizadeh, M., Chow, A.-H.-L., Fairbrother, J.E., 1984. Non-linear van't Hoff solubility-temperature plots and their pharmaceutical interpretation. Int. J. Pharm. 18, 25–38. https://doi.org/10.1016/0378-5173(84)90104-2.

Carrero, J.I., 2024. Application of the van't Hoff equation to phase equilibria. ChemTexts 10, 4. https://doi.org/10.1007/s40828-024-00188-x.

Seeger, M., 2004. Gaussian processes for machine learning. Int. J. Neural Syst. 14, 69–106. https://doi.org/10.1142/S0129065704001899.

Deringer, V.L., Bartók, A.P., Bernstein, N., Wilkins, D.M., Ceriotti, M., Csányi, G., 2021. Gaussian Process Regression for Materials and Molecules. Chem. Rev. 121, 10073–10141. https://doi.org/10.1021/acs.chemrev.1c00022.

C.E. Rasmussen, Gaussian Processes in Machine Learning, in: 2004: pp. 63–71. https://doi.org/10.1007/978-3-540-28650-9_4.

Abranches, D.O., Maginn, E.J., Colón, Y.J., 2024. Stochastic machine learning via sigma profiles to build a digital chemical space. In: Proceedings of the National Academy of Sciences. https://doi.org/10.1073/pnas.2404676121.

Duvenaud, D., 2014. Automatic model construction with Gaussian processes. Apollo - University of Cambridge Repository. https://doi.org/10.17863/CAM.14087.

Matthews, A.de G., van der Wilk, M., Nickson, T., Fujii, K., Boukouvalas, A., León-Villagrá, P., Ghahramani, Z., Hensman, J., 2017. A Gaussian Process Library using TensorFlow. J. Mach. Learn. Res. 18, 1–6. http://jmlr.org/papers/v18/16-537.html.

Martín Abadi, Ashish Agarwal, Paul Barham, Eugene Brevdo, Zhifeng Chen, Craig Citro, Greg S. Corrado, Andy Davis, Jeffrey Dean, Matthieu Devin, Sanjay Ghemawat, Ian Goodfellow, Andrew Harp, Geoffrey Irving, Michael Isard, Y. Jia, Rafal Jozefowicz, Lukasz Kaiser, Manjunath Kudlur, Josh Levenberg, Dandelion Mané, Rajat Monga, Sherry Moore, Derek Murray, Chris Olah, Mike Schuster, Jonathon Shlens, Benoit~Steiner, Ilya Sutskever, Kunal Talwar, Paul Tucker, Vincent Vanhoucke, Vijay Vasudevan, Fernanda Viégas, Oriol Vinyals, Pete Warden, Martin Wattenberg, Martin Wicke, Yuan Yu, Xiaoqiang Zheng, TensorFlow: Large-Scale Machine Learning on Heterogeneous Systems, (2015). https://www.tensorflow.org/.

Byrd, R.H., Lu, P., Nocedal, J., Zhu, C., 1995. A limited memory algorithm for bound constrained optimization. SIAM J. Sci. Comput. 16, 1190–1208. https://doi.org/10.1137/0916069.

T. Tadros, Critical Micelle Concentration, in: Encyclopedia of Colloid and Interface Science, Springer Berlin Heidelberg, Berlin, Heidelberg, 2013: pp. 209–210. https://doi.org/10.1007/978-3-642-20665-8_60.

Khoshnood, A., Lukanov, B., Firoozabadi, A., 2016. Temperature Effect on Micelle Formation: Molecular Thermodynamic Model Revisited. Langmuir 32, 2175–2183. https://doi.org/10.1021/acs.langmuir.6b00039.

Shimizu, S., Chan, H.S., 2000. Temperature dependence of hydrophobic interactions: A mean force perspective, effects of water density, and nonadditivity of thermodynamic signatures. J Chem Phys 113, 4683–4700. https://doi.org/10.1063/1.1288922.

Southall, N.T., Dill, K.A., Haymet, A.D.J., 2002. A View of the Hydrophobic Effect. J. Phys. Chem B 106, 521–533. https://doi.org/10.1021/jp015514e.

Kronberg, B., Castas, M., Silvestonti, R., 1994. Understanding the Hydrophobic Effect. J. Dispers. Sci. Technol. 15, 333–351. https://doi.org/10.1080/01932699408943561.

Swiatla-Wojcik, D., Pabis, A., Szala, J., 2008. Density and temperature effect on hydrogen-bonded clusters in water - MD simulation study. Open Chem. 6, 555–561. https://doi.org/10.2478/s11532-008-0059-7.

Dougherty, R.C., 1998. Temperature and pressure dependence of hydrogen bond strength: a perturbation molecular orbital approach. J. Chem. Phys. 109, 7372–7378. https://doi.org/10.1063/1.477343.

Gomes, R.J., Kumar, R., Fejzić, H., Sarkar, B., Roy, I., Amanchukwu, C.V., 2024. Modulating water hydrogen bonding within a non-aqueous environment controls its reactivity in electrochemical transformations. Nat. Catal. 7, 689–701. https://doi.org/10.1038/s41929-024-01162-z.

Andanson, J.-M., Bordes, E., Devémy, J., Leroux, F., Pádua, A.A.H., Gomes, M.F.C., 2014. Understanding the role of co-solvents in the dissolution of cellulose in ionic liquids. Green Chem. 16, 2528. https://doi.org/10.1039/c3gc42244e.

Abranches, D.O., Benfica, J., Shimizu, S., Coutinho, J.A.P., 2020. Solubility Enhancement of Hydrophobic Substances in Water/Cyrene Mixtures: A Computational Study. Ind. Eng. Chem. Res. 59, 18247–18253. https://doi.org/10.1021/acs.iecr.0c03155.

Morgado, P., Barras, J., Duarte, P., Filipe, E.J.M., 2020. Solubility of water in n-alkanes: New experimental measurements and molecular dynamics simulations. Fluid Phase Equilib. 503, 112322.